Journal of Molecular Liquids 303 (2020) 112598

Contents lists available at ScienceDirect

Journal of Molecular Liquids

journal homepage: www.elsevier.com/locate/molliq

Flexible bond and angle, FBA/ϵ model of water

Raúl Fuentes-Azcatl[a,*], Marcia C. Barbosa[b]

[a] UNAM, México 04000, Mexico
[b] Instituto de Física, Universidade Federal do Rio Grande do Sul, Caixa Postal 15051, CEP 91501-970 Porto Alegre, RS, Brazil

ARTICLE INFO

Article history:
Received 4 June 2019
Received in revised form 25 January 2020
Accepted 26 January 2020
Available online 30 January 2020

ABSTRACT

We propose a new flexible force field of water, from the parameters of the SPC/ϵ model. The model includes, in addition to the Lennard-Jones and electrostatic parameters, the flexibility in O—H bonds and angle. The parameters are the result of the optimization in order to reproduce the experimental values of the density and dielectric constant of water at 1 bar and 240 K using the dipole moment of minimum density method "$\mu_{\min\rho}$" and the infrared spectrum as a experimental data target to obtain the harmonic potential parameters of the bond and angle. The FBA/ϵ reproduces the experimental values of structural, thermodynamic and the phase behavior of water in a wide range of temperatures that improve the three sites non-polarizable models and the flexible models with the same form of potential.

1. Introduction

Water is ubiquitous in nature and strongly affects other materials when is in solution. This simple molecule, two hydrogen atoms linked to the oxygen by a covalent bond. In gas phase, the H—O—H angle is 104, 474° and the distance between oxygen and each hydrogen in 0.095718 nm [1]. This angular structure is not fixed. In the liquid phase at 298 K and 1 bar, it reaches the angle of 106° [2]. Since the electrons in the covalent H—O bond are strongly attracted to the oxygen, water is polarized with the region of the oxygen negative and the region of the hydrogen positive. Consequently, the oxygen of one water attracts the hydrogen of the other water molecule forming the hydrogen bonding. Water due to the H—O—H angular structure can form up to four hydrogen bonds what leads to the tetrahedral structure which can aggregate in octamers. Then, a small angular difference in the H—O—H covalent bonds can be relevant to the cluster structure of water.

In order to give a description of thermodynamic and dynamic properties of water for a certain range of temperatures and pressures, a number of non-polarizable models have been developed. The idea is to adjust the interaction potential between the molecules, so the simulations reproduce the experimental value of a property such as the density at a certain temperature and pressure. This process has generated rigid models, manageable computationally, which give accurate values for a wide range of thermodynamic and dynamic functions. However, since the potentials are fitted at a specific pressure and temperature, they are not able to cover different thermodynamic phases.

The rigid models are unable to capture the changes in the water polarization due to variations in temperature and pressure, these models lack physics-electronic polarizability. Even a fixed-charge rigid model that reproduces most bulk liquid properties exactly, would be inherently incapable to respond properly to the change of polarity of its nano-states. Taking into account, the harmonic potential adds a type of polarization in the molecule [6].

This becomes particularly problematic when water is mixed with ionic or hydrophilic solutes. For instance, the rigid models do not reproduce the increase of the excess of specific heat when alcohol is added to water and they are unable to explain the enhancement of the self-diffusion of water in the presence of certain electrolytes [4]. From the desire to produce an atomistic model which accounts for changes in the H—O—H water angle, without the computational costs of the ab initio simulations, a number of flexible models were introduced. Some of them were based in original non-polarizable models such as the SPC/E [5] and the TIP4P/2005 [6] with the addition of more degrees of freedom. With this new approach, accurate water transport and other thermophysical properties were obtained [5-8,13], however, these models fail in reproduce other thermodynamic and dynamic properties [5,13]. For instance, they do not give good estimates of the charge distribution [5,9-12]. Therefore, a good flexible model is still missing.

In this work, we address this issue by following the same strategy adopted by Wu et al. [5] and Gonzalez and Abascal [6] by starting with a rigid non-polarizable model, in our case the SPC/ϵ [14] model and by introducing flexible bonds and angles. The idea is to combine

* Corresponding author.
E-mail addresses: razcatl@xanum.uam.mx (R. Fuentes-Azcatl), marcia.barbosa@ufrgs.br (M.C. Barbosa).

https://doi.org/10.1016/j.molliq.2020.112598
0167-7322/

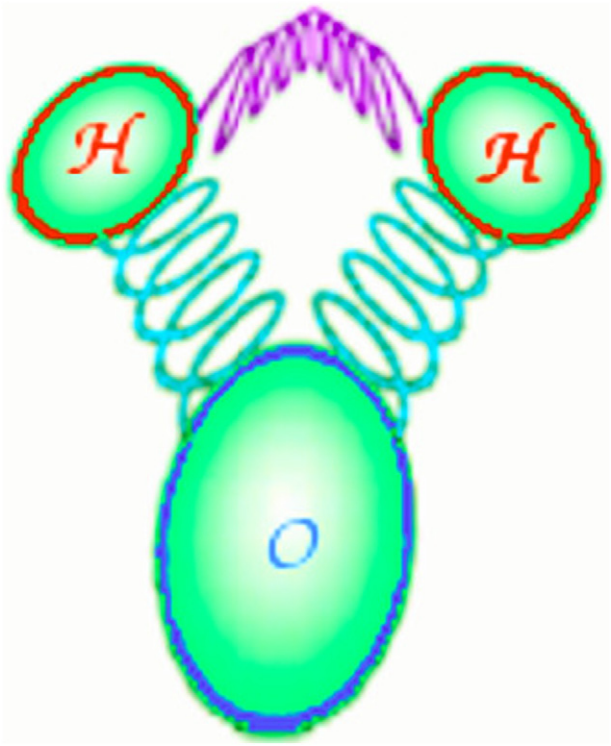

Fig. 1. Model of water including the harmonic potential in bonds and angle.

the parametrization strategy designed by Fuentes et al. [14,18] with the flexibility in order to add additional degrees of freedom for the parametrization. We selected the rigid SPC/ϵ [14] as a starting point due to its simplicity and because the rigid model already gives some thermodynamic [14] and dynamic properties [16] close to the experimental results at room temperature and pressures.

The paper is organized as follows: Section 2 introduces the force field of FBA/ϵ model of water, Section 3 compares the results for the thermodynamic and dynamic properties obtained with the FBA/ϵ with results obtained by non-polarizable models and experimental values. Section 4 ends the paper with conclusions.

2. The FBA/ϵ force field

The Flexible Bond and Angle (FBA/ϵ) model is illustrated in Fig. 1. The molecule is represented by three sites. The oxygen attracts more electrons and therefore has a negative charge while the hydrogens have the positive charges. The bonds and angles are not fixed, but oscillate and are represented by a harmonical potentials, the use of these help to improve the reproduction of many experimental values as recently did Fuentes et al. [17]. The interaction potential contains the following contributions

$$U(r) = U_{LJ}(r) + U_e + U_k(r) + U_\theta \ . \tag{1}$$

In Eq. (1), U_{LJ}, the Lennard-Jones term, describes the intermolecular interactions between the massive particles, the oxygens, and it is given by

$$U_{LJ}(r) = 4\epsilon_{\alpha\beta}\left[\left(\frac{\sigma_{\alpha\beta}}{r}\right)^{12} - \left(\frac{\sigma_{\alpha\beta}}{r}\right)^{6}\right] \tag{2}$$

where r is the distance between the oxygens of two neighbor molecules α and β, $\epsilon_{\alpha\beta}$ is the LJ energy scale and $\sigma_{\alpha\beta}$ the repulsive diameter for an $\alpha\beta$ pair. The cross interactions are obtained using the Lorentz-Berthelot mixing rules,

$$\sigma_{\alpha\beta} = \left(\frac{\sigma_{\alpha\alpha} + \sigma_{\beta\beta}}{2}\right); \epsilon_{\alpha\beta} = (\epsilon_{\alpha\alpha}\epsilon_{\beta\beta})^{1/2} \ . \tag{3}$$

The Coulomb forces between the oxygens and hydrogens are represented by

$$U_e(r) = \frac{1}{4\pi\epsilon_0}\frac{q_\alpha q_\beta}{r} \tag{4}$$

where r is the distance between sites α and β, $q_\alpha(\beta)$ is the electric charge of site $\alpha(\beta)$ and ϵ_0 is the permittivity of vacuum.

The difference between the rigid SPC/ϵ and the FBA/ϵ model is the introduction in the same molecule the intramolecular harmonic potentials in the bonds

$$U_k(r) = \frac{k_r}{2}(r - r_0)^2 \tag{5}$$

and in the angle. In order to improve the intermolecular interaction by adding these degrees of freedom, the molecules can deform according to the interaction with other molecules. The value of these new parameters was obtained based on the reproduction of the infrared power spectrum that experimentally describes this behavior, mainly the best reproduction of the IR spectrum of bending H—O—H help to improve the model. Table 2

$$U_\theta(\theta) = \frac{k_\theta}{2}(\theta - \theta_0)^2, \tag{6}$$

where r is the bond distance and θ is the bond angle. The subscript 0 denotes their equilibrium values, k_r and k_θ are the corresponding spring constants.

The model has the following parameters: $\epsilon_{\alpha\beta}$, $\sigma_{\alpha\beta}$, q_α, q_β, r_0, θ_0, k_r and k_θ.

The parameterization procedure is the same employed in previous publication [18] and goes as follows: Based on the values of the SPC/ϵ model, the $\epsilon_{\alpha\beta}$, $\sigma_{\alpha\beta}$, q_α and q_β were defined in a first step and then we add the harmonical potential in bonds and angle with the values of SPC/Fw, this changed the $\mu_{\min\rho}$. Iteratively, we found the best set of values that would keep the $\mu_{\min\rho}$ and improve the reproduction of IR spectrum. Then, the procedure was using the $\mu_{\min\rho}$ method as a first step of parametrization, and a second step the reproduction of IR spectrum, until getting the best values for the new flexible model. The parameters of the model are illustrated in Table 1.

Table 1
Parameters of the three-site water models considered in this work.

Model	k_b	r_{OH}	k_a	Θ	ε_{OO}	σ_{OO}	q_O	q_H
	kJ/mol Å^2	Å	kJ/mol rad^2	deg	kJ/mol	Å	e	e
SPC/E [14]	–	1.000	–	109.45	0.650155	3.1660	−0.8476	0.4238
SPC/ϵ [14]	–	1.000	–	109.45	0.705859	3.1785	−0.8900	0.4450
OPC3 [15]	–	0.97888	–	109.47	0.68369	3.17427	−0.89517	0.447585
FBA/ϵ	3000	1.027	383	114.70	0.792324	3.1776	−0.8450	0.4225
SPC/Fw [5]	4236.648	1.012	317.56	113.24	0.650299	3.165492	−0.8200	0.4100

Table 2
Experimental and simulation data results of 3 sites water models. The thermodynamic conditions are reported according to the calculated property.

Property	Exp. data	SPC/Fw	SPC/ϵ	FBA/ϵ	OPC3	Tol. (%)	SPC/Fw score	SPC/ϵ score	FBA/ϵ score	OPC3 score
Enthalpy of phase change/kcal mol^{-1}										
ΔH_{melt}	1.44	0.74	5.38	0.582	6.62	2	0	0	0	0
ΔH_{vap}	10.52	6.95	11.48	10.63	10.86	2	0	5.4	9.5	8.4
Critical point properties										
T_C/K	647.1	627	659.88	627.28	640.59	5	9.4	9.6	9.4	9.8
ρ_C/g cm^{-3}	0.322	0.31	0.3121	0.2854	0.2989	5	9.3	9.4	7.7	8.6
Surface tension/mN m^{-1}										
γ_{300K}	71.73	64.31	70.02	73.98	65.24	2	4.8	8.8	8.4	5.5
γ_{400K}	53.6	45.4	54.56	48.9	47.6	2	2.4	9.1	5.6	4.4
γ_{450K}	42.88	35.8	47	46.2	39.61	2	1.7	5.2	6.1	6.2
Melting properties										
T_m/K	273.15	215	200	251	215	2.5	0	0	6.8	1.5
ρ_{liq}/g cm^{-3}	0.999	1.011	0.9864	0.9946	0.996	0.5	7.6	7.5	9.1	9.4
ρ_{sol}/g cm^{-3}	0.917	0.95	0.89	0.94	0.9481	0.5	2.8	4.1	5.0	3.2
Orthobaric densities and temperature of maximum density **TMD**										
TMD/K	277	257.5	266	275.4	265	1	3.0	6.0	9.4	5.7
ρ_{260K}/g cm^{-3}	0.9969	1.0206	1.0006	0.9964	1.00063	0.5	5.2	9.3	9.9	9.3
ρ_{298K}/g cm^{-3}	0.997	1.0101	0.9964	0.9948	0.9961	0.5	7.4	9.9	9.6	9.8
ρ_{400K}/g cm^{-3}	0.9375	1.05	0.9385	0.9406	0.9261	0.5	0.0	9.8	9.3	7.6
ρ_{450K}/g cm^{-3}	0.8903	0.933972	0.889287	0.8982	0.8758	0.5	0.2	9.8	8.2	6.7
Isothermal compressibility/10^{-}6 bar^{-1})										
κ_T [1 bar; 298 K]	45.3	16.87	41.4	45.6	43.6	1	0	1.4	9.3	6.2
κ_T [1 bar; 318 K]	44.25	15.52	42.24	43.9	45.3	1	0	5.5	9.2	7.6
κ_T [1 bar; 360 K]	47	14.24	46.96	47.1	51.3	1	0	9.9	9.8	0.9
Thermal expansion coefficient/10^5 K^{-1})										
α_P [1 bar; 298 K]	22.66	5.1	24.71	25.3	35.36	5	0	8.2	7.7	0.0
α_P [1 bar; 350 K]	68.2	18.67	62.56	71.1	68.11	5	0	8.3	9.1	10.0
Gas properties										
ρ_v[350 K] (bar)	0.417	1.7058	0.042	0.224	0.38	5	0	0	0.7	8.2
ρ_v[450 K] (bar)	9.32	7.69	1.88	5.42	3.83	5	6.5	0	1.6	0.0
Static dielectric constant										
ε[liq; 298 K]	78.5	80.18	78.3	75.5	79.74	1	7.9	9.7	6.2	8.4
ε[liq; 350 K]	62.12	63.97	64.65	61.49	65.3395	1	7.0	5.9	9.0	4.8
ε[10 kbar, 300 K]	103.63	101.49	106.65	104.9	109.237	1	7.9	7.1	8.8	4.6
T_m-TMD-T_c. ratios										
$T_m[I_h]/T_c$	0.422	0.3429	0.303	0.4001	0.3356	5	6.3	4.4	9.0	5.9
TMD/T_c	0.428	0.4106	0.403	0.4390	0.4136	5	9.2	8.8	9.5	9.3
TMD-T_m (K)	4	42.5	66	24.4	50	5	0	0	0	0.0
Densities of ice polymorphs/g cm^{-3}										
$\rho[I_h$ 250 K; 1 bar]	0.92	0.944	0.997	0.931	0.938	0.5	4.8	0	7.6	6.1
ρ[II 123 K; 1 bar]	1.19	1.245	1.166	1.22	1.245	0.5	0.8	6.0	5.0	0.8
ρ[V 223 K; 5.3 kbar]	1.283	1.294	1.273	1.294	1.295	0.5	8.3	8.4	8.3	8.1
ρ[VI 225 K; 11 kbar]	1.373	1.403	1.33	1.403	1.403	0.5	5.6	3.7	5.6	5.6
EOS high pressure										
ρ[373 K; 10 kbar]	1.201	1.2222	1.2034	1.215	1.2049	0.5	6.5	9.6	7.7	9.4
ρ[373 K; 20 kbar]	1.322	1.346	1.3219	1.339	1.3255	0.5	6.4	10.0	7.4	9.5
Self-diffusion coefficient/cm^2 s^{-1}										
ln D_{278K}	−11.24	−11.35	−11.69	−11.58	−11.31	1	9.0	6.0	7.0	9.4
ln D_{298K}	−10.68	−10.77	−11.08	−11.01	−10.76	1	9.2	6.3	6.9	9.3
E_a k$_J$ mol^{-1}	18.4	15.4	17.82	15.98	16.61	5	6.7	9.4	7.4	8.1
Shear viscosity/mPa s										
η[1 bar; 298 K]	0.896	0.729	1.259	1.265	0.771	5	6.3	1.9	1.8	7.2
η[1 bar; 373 K]	0.284	0.269	0.378	0.364	0.271	5	8.9	3.4	4.4	9.1

(*continued on next page*)

Table 2 (*continued*)

Property	Exp. data	SPC/Fw	SPC/ϵ	FBA/ϵ	OPC3	Tol. (%)	SPC/Fw score	SPC/ϵ score	FBA/ϵ score	OPC3 score
Power spectrum-wavenumbers (cm^{-1}) [1 bar; 298 K]										
Cage vibrations	50	50	0	50	0	2	10.0	0	10.0	0
Intermolecular stretch	183.4	278	0	278	0	2	0.0	0	0.0	0
Librations A2	430	513	0	536	0	2	0.3	0	0.0	0
Librations B2	650	675	0	685	0	2	8.1	0	7.3	0
Bending (H—O—H)	1643.5	1500	0	1613	0	2	5.6	0	9.1	0
Stretching (O—H)	3404	3742	0	3060	0	2	5.0	0	4.9	0
Overall score (out of 10)							4.5	5.4	6.9	5.6

3. Simulation details

We performed molecular dynamics simulations in the isothermal-isobaric ensemble, NPT, with isotropic fluctuations of volume, to compute the liquid properties at different temperatures and pressures, 1 bar. These simulations involved typically 500 molecules.

In order to compute the surface tension, we used the constant volume and temperature ensemble, NVT, and 5832 molecules. We obtained the liquid-vapor interface by setting up a liquid slab surrounded by vacuum in a simulation box with periodic boundary conditions in the three spatial directions. The dimensions of the simulation cell were $Lx = Ly = 54$u Å with $Lz = 3Lx$, with z being the normal direction to the liquid-vapor interface. The GROMACS 4.5.4 package [19,20] was employed in all simulations presented in this work. The equations of motion were solved using the leapfrog algorithm with a time step of 1 fs. The temperature was coupled to the Nosé-Hoover thermostat with a parameter $\tau_T = 0.2$ ps while the pressure was coupled to the Parrinello-Rahman barostat [21]with a coupling parameter $\tau_P = 0.5$ ps.

We computed the electrostatic interactions with the particle mesh Ewald approach [22] with a grid spacing of 1.2 Å and spline

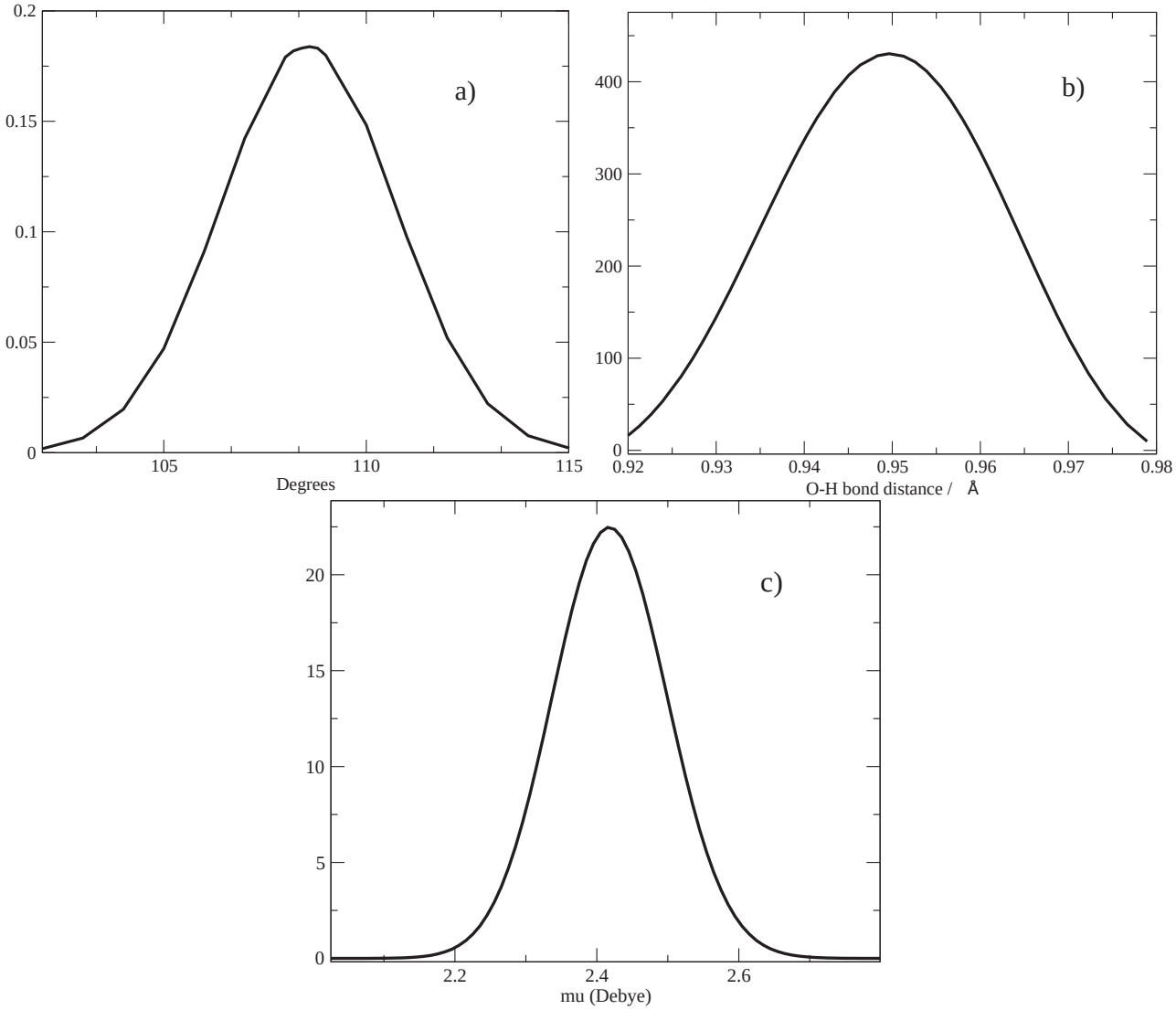

Fig. 2. (a) H—O—H angle, (b) O—H bond distance, (c) dipole moment distributions at 298 K and 1 bar for the FBA/ϵ model.

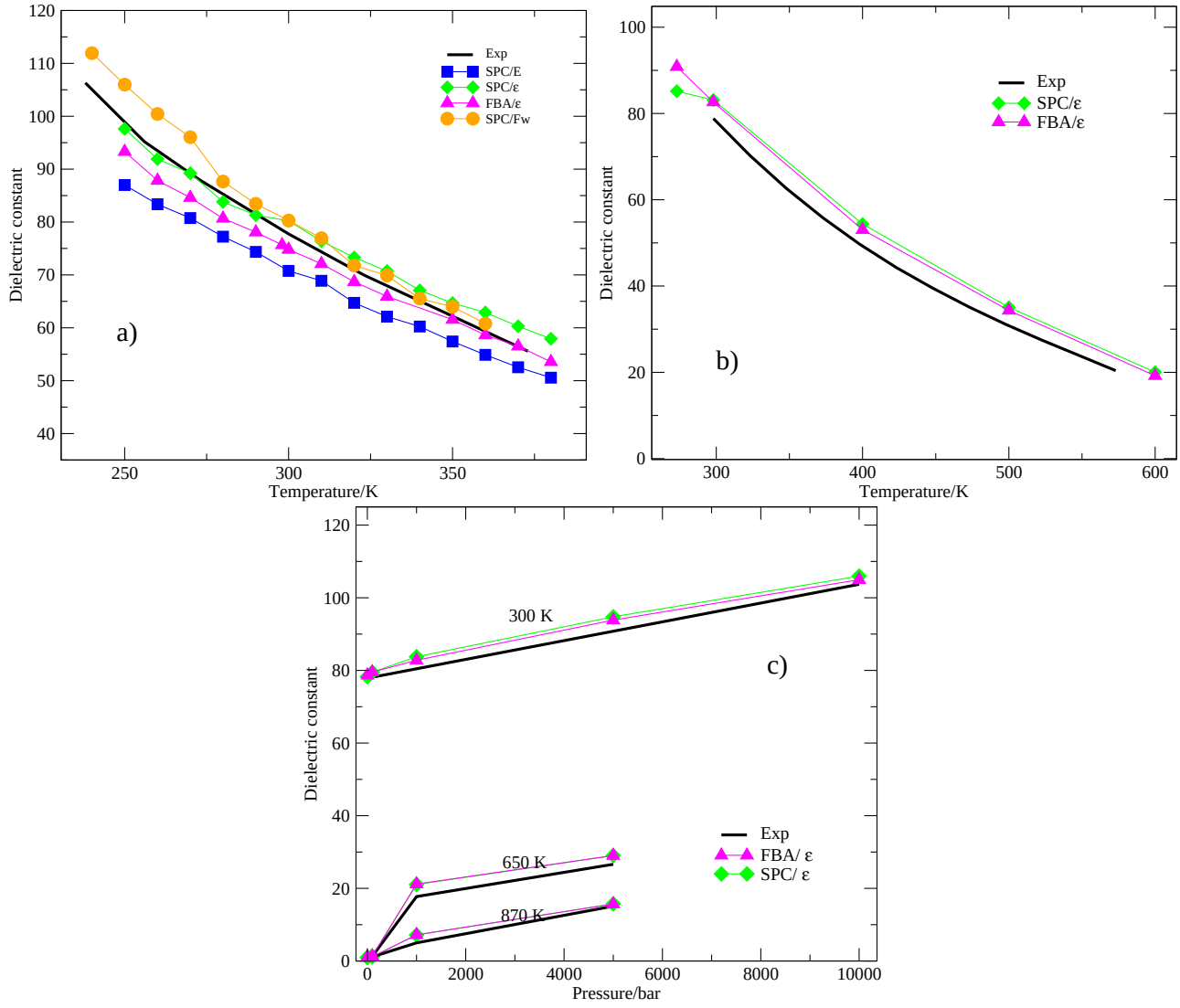

Fig. 3. (a) Dielectric constant (a) versus temperature at 1 bar, (b) versus temperature at the liquid-vapor coexistence line and (c) versus pressure for three different temperatures for SPC/E [14] (squares), SPC/ϵ [14] (diamonds), FBA/ϵ (triangles), SCP/Fw (circles) models and experimental data [34] (solid line).

interpolation of order 4. In the isotropic NPT simulations, the real part of the Ewald summation and the LJ interactions were truncated at 9 Å. Long range corrections for the LJ energy and pressure were included. The dielectric constant is obtained from the analysis of the dipole moment fluctuations of the simulation system [23,24]. The density and the dielectric constant were calculated from the same simulation for at least 200 ns after an equilibration period of 10 ns. For the surface tension computations in the NVT ensemble, the cutoff was set to 26 Å, since the surface tension depends on the truncation of the interactions [25] and the interface cross-sectional area [26,27]. The equilibration period for the interfacial simulations was 2 ns, and the results for the average properties were obtained over an additional 10 ns trajectory.

For the calculation of the density of the solid phases here reported (ice Ih, II, V, VI), we have carried out isothermal-isobaric(NpT) simulations. For the initial configurations, we used the structural data obtained from diffraction experiments. The NpT simulations are performed under periodical boundary conditions at 1 fs and 2 fs without seeing any change in density and at 10 ns. The Berendsen thermostat and barostat were used with parameters of 0.2 and 0.5 ps, respectively. The different phases are identified by the radial distribution function and snapshots. The more stable phase is the selected by comparing the energies and starting the simulations in one phase and decreasing and increasing the temperature.

The Berendsen barostat was employed for the calculation of the melting temperature and of the density of the ice. The use of this barostat allows the simulation box to expand or contract, and then to form ice or liquid phases. For studying the ice phase and the melting properties, the temperature was fixed with a Berendsen thermostat with a relaxation time of 0.2 ps [28]. For the description of the coexistence between liquid and solid water, we employed an orthogonal cell. This approach is consistent with the crystallographic data of the solid phase Ih [29]. The cell size is $Lx = 21.6$ Å, $Ly = 23.3$ Å and $Lz = 53.8$ Å, which gives us a contact area between the $Lx * Ly = 503.28$ Å^2 phases.

4. Results

First, we analyzed the water structure obtained using our model. Differently from the rigid models, the FBA/ϵ exhibits a distribution of H—O—H angles illustrated for 1 bar and 298 K in Fig. 2 (a). The

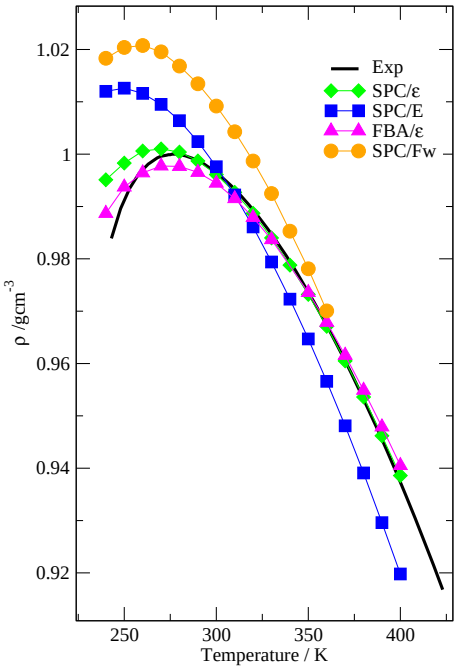

Fig. 4. Density as a function of temperature at 1 bar for the SPC/E [14] (squares), SPC/ϵ [14] (diamonds), FBA/ϵ (triangles), SCP/Fw calculated here (circles) models and experimental data [34] (solid line).

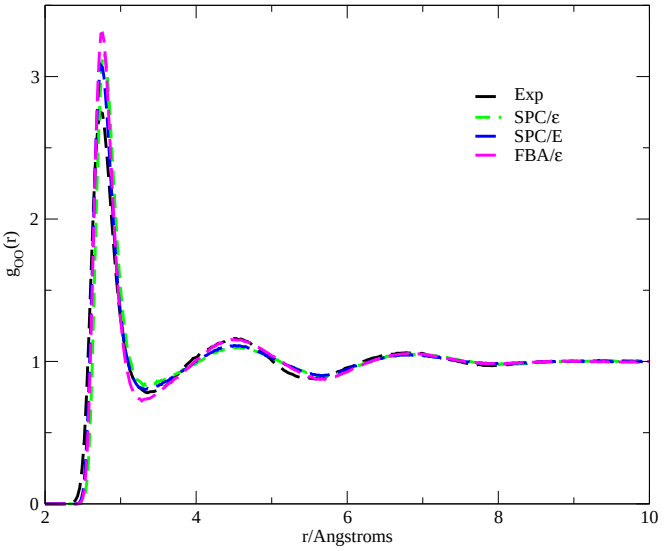

Fig. 5. Oxygen-oxygen pair distribution function for the SPC/E [14] (green), SPC/ϵ [14] (blue), FBA/ϵ (magenta) models at 298 K and 1 bar. (For interpretation of the references to color in this figure legend, the reader is referred to the web version of this article.)

average angle, 108.56° is close to the average experimental value [2] which is 106° and to the value employed for the rigid SPC model which is 109.47°. The distribution of O—H bond distances for the FBA/ϵ model at 298 K and 1 bar is illustrated in Fig. 2 (b). This result shows the average bond distance at of 0.09495 nm that is 4% lower than the neutron diffraction value, 0.099 nm [30], and only 2.4% lower than the X-ray diffraction value, 0.09724 nm [31,32]. In principle, rigid models can be constructed to give this bond distance, however, they cannot accommodate the change with the temperature of the O—H bond distance observed both in the experiments and in our model. Fig. 2 (c) shows the distribution of dipole moments of the water molecules at 298 K and 1 bar. The mean dipole moment of the distribution is 2.42 D.

Next, we tested how robust is the parametrization regarding variations of temperature. The flexible FBA/ϵ and the SPC/ϵ models were parametrized to reproduce the experimental value of the dielectric constant, ϵ, at 240 K and 1 bar [18] with a 3.6% of tolerance [35]. Fig. 3 illustrates the dielectric constant in three different conditions: versus temperature at 1 bar, versus temperature at the liquid-vapor coexistence and versus pressure at different temperatures. The comparison indicates that SPC/ϵ and the FBA/ϵ both give very reliable results for a wide range of pressures and temperatures for the dielectric constant.

The reproduction of the density at 1 bar at different pressures of the FBA/ϵ was calculated and the model reproduces the experimental density at 298 K and 1 bar [34] with an error of 0.22%. Fig. 4 shows the density as a function of the temperature for the FBA/ϵ, SPC/E [14], SPC/ϵ [14], SPC/*Fw* [5] models and the experiments [34]. The SPC/ϵ and the FBA/ϵ agree with the experiments at 298 K since they were not parametrized to give the correct density at this temperature. The SPC/E [14], however, at low temperatures overestimates the density, while both the SPC/ϵ [14] and FBA/ϵ agree with the experiments for

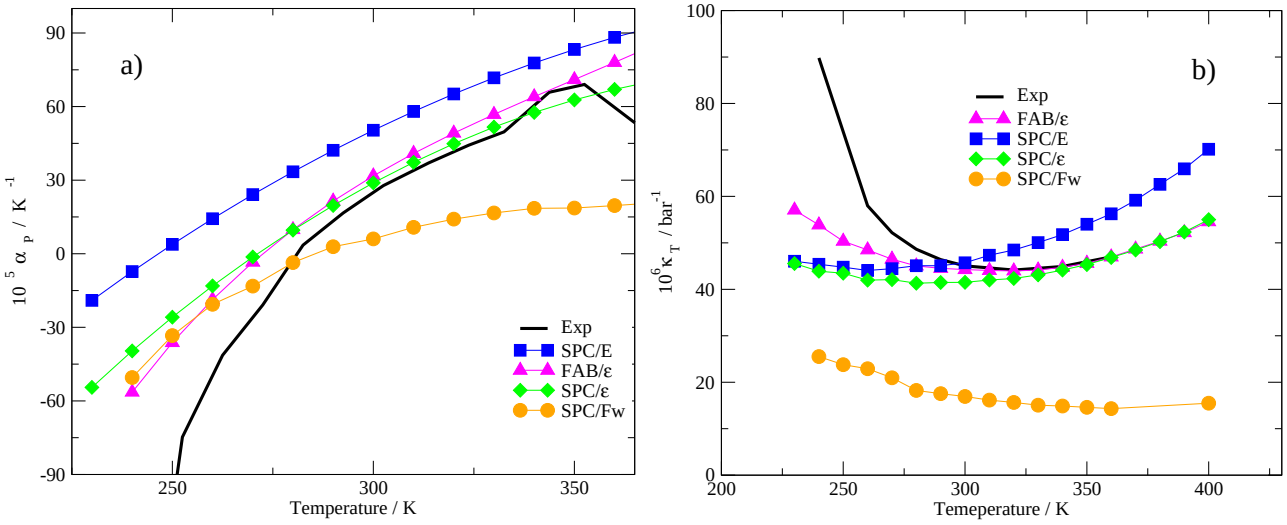

Fig. 6. (a) Thermal expansion coefficient and (b) isothermal compressibility as a function of temperature at pressure constant of 1bar for the SPC/E [14] (squares), SPC/ϵ [14] (diamonds), FBA/ϵ (triangles), SCP/Fw calculated here (circles) models and experimental data [34] (solid line).

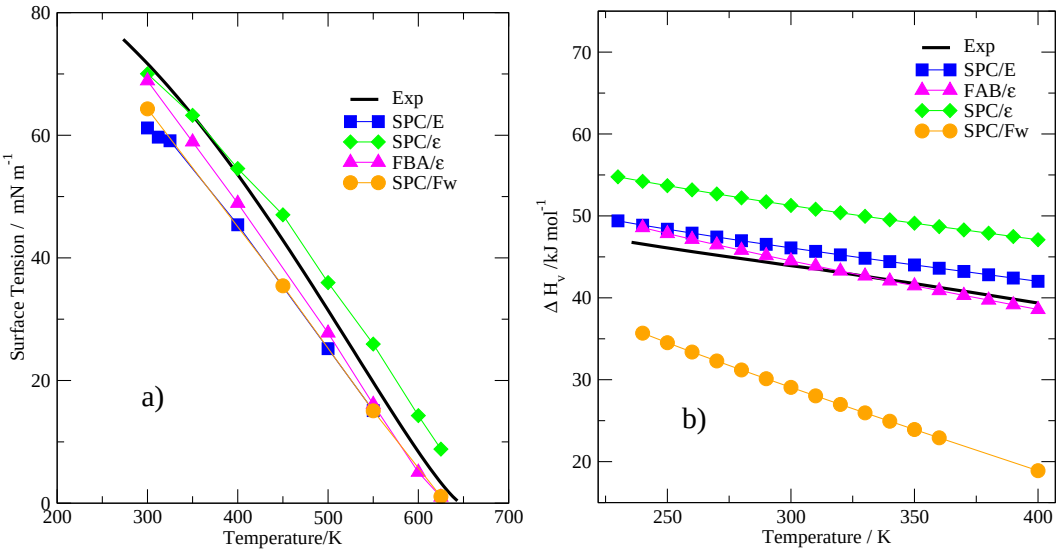

Fig. 7. (a) Surface tension and (b) heat of vaporization as a function of temperature at pressure constant of 1bar for the SPC/E [14] (squares), SPC/ϵ [14] (diamonds), FBA/ϵ (triangles), SCP/Fw calculated here (circles) models and experimental data [34] (solid line).

a wide range of temperatures. The FBA/ϵ at very low temperatures shows an improvement over the SPC/ϵ [14] model.

The radial distribution function $g(r)$ reflects the average liquid structure around a central atom. Fig. 5 shows the oxygen-oxygen radial distribution function for simulations at 298 K and 1 bar. The three sites models give the first and second picks with the same height and position but higher than experimental data. This result indicates that the effective interoxygen attraction for two neighboring oxygen atoms is increased by longer O—H bonds [5].

Then, we explore the behavior of the functions which are not linked with the parametrization procedure. If the model would be robust, even response functions would be reproducible. Response functions exhibit a very peculiar behavior in water. The thermal expansion coefficient, α, which for most materials is almost constant or slightly increases with the temperature, for water it decreases abruptly with the decrease of the temperature and it becomes negative and the new model presents better behavior at different temperatures. The compressibility for a number of materials increases monotonically with the temperature, but in the case of water, it has a minimum and the new model capture the minimum. Fig. 6 illustrates both α and κ_T as a function of temperature for SPC/E, SPC/ϵ, FBA/ϵ models and the experimental results [34]. At low temperatures, all models do not reproduce the values α and κ_T, but from values close to 300 K and at higher temperatures, the new flexible model FBA/ϵ reproduces the experimental data of κ_T and in the case of the α around 350 K reproduces the experimental data.

In the particular case of the compressibility, the flexible model shows the minimum approximately in the same temperature as the experiments, while the non-polarizable force fields present a shift.

Even though the model was parametrized at the liquid phase, we check if the flexible model also presents a good agreement with the experiments for high temperatures at the vapor phase. One important property in which the flexibility might matter is the surface tension. For testing the behavior at high temperatures, we calculated the surface tension. The surface tension versus temperature is shown in Fig. 7 (a). The flexible model shows a consistent agreement with the experiment while the rigid models fit the data either at low or high temperatures but not for both ranges. As the

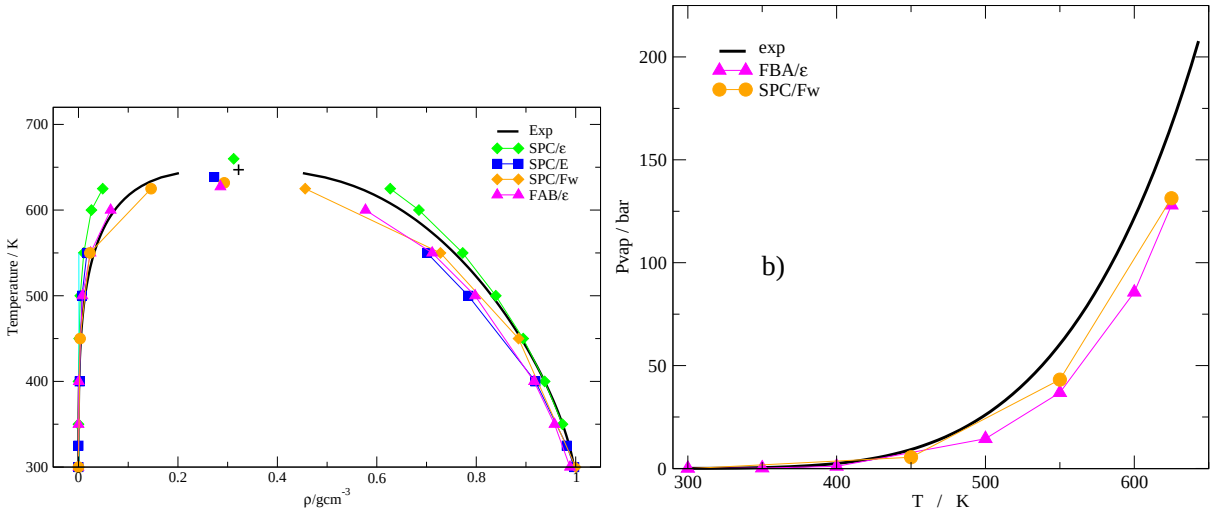

Fig. 8. Temperature versus density phase diagram for the SPC/E [14] (squares), SPC/ϵ [14] (diamonds), FBA/ϵ (triangles), SPC/Fw calculated here (circles) models and experimental data [34] (solid line).

temperature is increased, it is not clear how the H—O—H angle and the O—H bond might change. In order to check this, we look at the liquid-vapor transition. Fig. 7 (b) compares the heat of vaporization as a function of the temperature at 1 bar for the SPC/E [14] (squares), SPC/ϵ [14] (solid diamonds), FBA/ϵ (triangles) models with the experimental data [34] (solid line). It shows that flexible FBA/ϵ agrees with the data which suggests that the flexibility keeps the correct reproduction for the vapor heat specifically but might affect coexistence properties. In order to check this point, we also obtain the gas-liquid phase diagram. The coexisting densities were estimated from the average density profile in the liquid and vapor regions of the slab. Fig. 8 (a) shows the temperature versus density phase diagram for the SPC/E [14] (squares), SPC/ϵ [14] (diamonds), FBA/ϵ (triangles) models and experimental data [34] (solid line). The flexible model improves the agreement with experiment significantly compared to the rigid models for the gas phase and for the critical temperature and density. The vapor pressure is calculated as the normal component of the pressure tensor in the interface simulations, Fig. 8 (b) shows the reproduction of the vapor pressure at different temperatures compared with the experimental data [34].

To calculate the Infrared Spectrum IR, we did simulation with a short time of 10 ps, because of the rapid decay of the velocity autocorrelation function with a time-step, 0.1 fs. In Fig. 9, there are the results of the calculation of the IR of the SPC/Fw and the new FAB/ϵ flexible models of water, contrasting the bands of the experimental data [33].

In Fig. 9, both models reproduce the 50 cm^{-1} band and the 230 cm^{-1} band is underestimated by 34% for both models. The bands corresponding to the librational movement, with the symmetries A2, B2 are presented by a single band whose maximum appears approximately in the medium 513 cm^{-1} for the SPC/Fw and 542 cm^{-1} for the new FAB/ϵ model; the spectrum for the angle is underestimated by the SPC/Fw by 8.7% and the FAB improves its reproduction by having a difference of less than 2.6%. Finally, the calculation of the spectrum that generates the vibration of the O—H bond, is overestimated by the SPC/Fw by 11.9% and underestimated by the FAB by 8.2%. In Table 2, the values of the band for each model are shown.

4.1. Melting temperature

In this work, we are interested in the new force field that could be able to reproduce the solid phases of water and the melting temperature, T_m. The red line describes the behavior of the potential energy of the system when it turns into a liquid phase and the black line has an energetic decrease that indicates that there is an entire Ice Ih-transforming system. The result of T_m is estimated to be 251 $\pm$ 0.5 K (Fig. 10). This result improved the 3 sites rigid non-polarizable models and the models that include flexibility 2, any is close to reproduce this value [9]. To calculate this property using direct coexistence simulations [36], anisotropic NPT simulations, starting from the same initial configuration, at 1 bar and temperatures ranging from 245 to 255 K is carried out on systems containing 870 water molecules in an elongated simulation cell in the z direction, half in the liquid and half in the ice Ih. The procedure is observing the melting or freezing by inspection of the total energy, if the system is above the T_m, the ice region will melt, but if the water is at a temperature below the melting point, the liquid water will be ice Ih [36] (Fig. 10).

4.2. Oxygen-oxygen pair distribution function of ice Ih

It has been shown that the relative stability of the ice polymorphs is not correctly predicted by the 3 sites rigid non-polarizable models such as TIP3P, SPC/E [9,37]. The new force field FAB/ϵ is stable for different phases of ice and improve the 3 sites rigid model non-polarizables, Table 2. The oxygen−oxygen pair distribution function obtained in NPT simulations at T = 240 K and P = 1 bar for solid Ih water is shown in the Fig. 11. A solid phase is unstable, when simulating, the solid phase becomes a liquid during the process or when the temperature varies within a range of one or more units of temperature. Further analysis of the solid phase for a more wide range of pressures and temperatures will be provided in a future publication.

Finally, a comprehensive comparison between the results obtained by our flexible model compared with its non-polarizable approaches is presented in the Table 2. Following the notation introduced by Vega et al. [9], the models are evaluated by a score. The final score of the FBA/ϵ is higher than the non-polarizable models of three sites.

There are two successful methods for the optimization of the rigid water molecule, which are the $\mu_{\min\rho}$ method proposed by Fuente-Azcatl et al. [18] and the Optimal Point Charge, OPC method, proposed by Izadi et al. [15]. Both methods improve the three sites rigid water models, but still have deficiencies; the new FAB/ϵ model that is developed using $\mu_{\min\rho}$ method and infrared spectrum as a target to optimize the values of the harmonic potential, improved

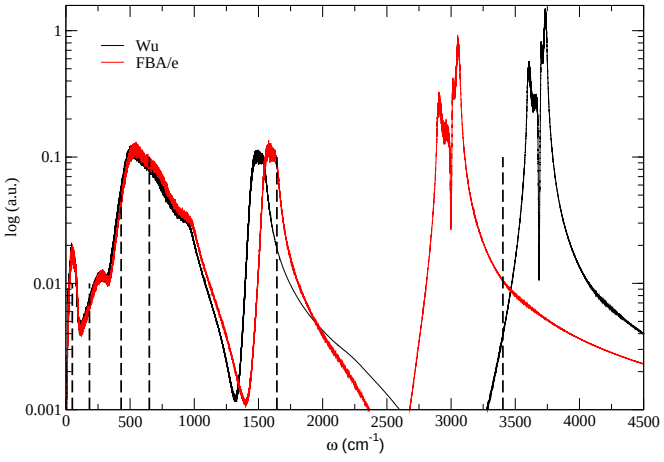

Fig. 9. The black line corresponds to FBA/ϵ and the red line corresponds to SPC/Fw model. The vertical dashed lines represent the experimental bands of the IR spectrum [33]. (For interpretation of the references to color in this figure legend, the reader is referred to the web version of this article.)

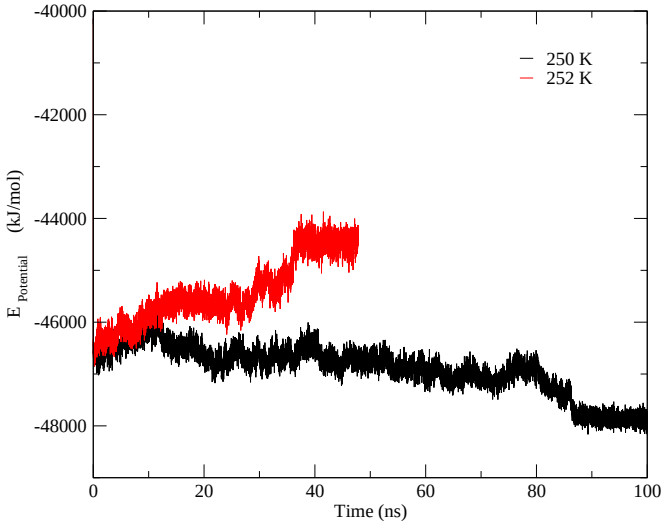

Fig. 10. Total energy of a water system vs time, between liquid water in contact with ice Ih. The results are NpT simulation runs at 1 bar and T = 250 K and 252 K. (For interpretation of the references to color in this figure, the reader is referred to the web version of this article.)

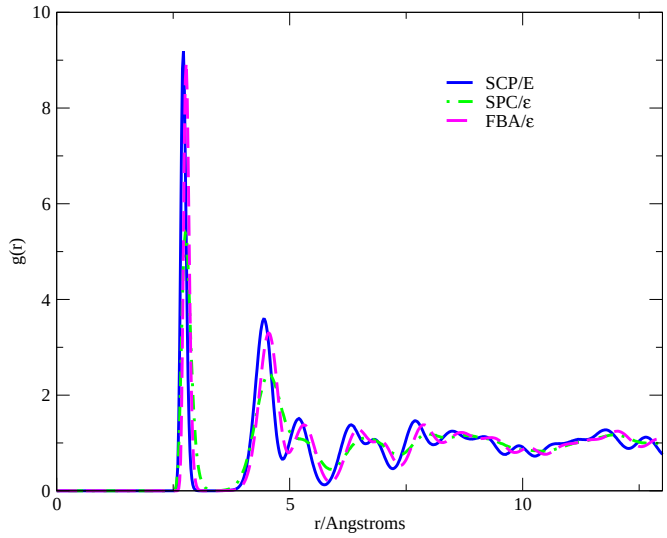

Fig. 11. Oxygen-oxygen pair distribution function of ice Ih at 240 K, for the SPC/E [14] (blue), SPC/ϵ [14] (green), FBA/ϵ (magenta). (For interpretation of the references to color in this figure legend, the reader is referred to the web version of this article.)

all the three sites rigid non-polarizable and flexible (with the same potential form) models of water.

5. Conclusions

We introduced a new 3 sites flexible model, the FBA/ϵ which was parametrized using the experimental values of the density, the dielectric constant using the dipole moment of minimum density method at 1 bar and 240 K and the reproduction of the IR spectrum, mainly the correct reproduction of the spectrum bending H—O—H, helped to improve the model.

This approach gives a bond and angle distribution compared with experimental results. It is also able to produce good agreement with the experiments for thermodynamic and structural properties at low and high temperatures. In particular, the flexibility allows the model to provide a good coexistence region of the density versus temperature phase diagram. The major advantage of the model is that it is able to reproduce with accuracy a wide range of properties at different temperatures. This robust behavior makes it a good candidate for studying mixtures of water and other polar materials.

Acknowledgments

We thank the Brazilian agencies CNPq,INCT-FCx, andCAPES for the financial support. We also thank the SECITI of Mexico City for financial support.

Appendix A. Supplementary data

Supplementary data to this article can be found online at https://doi.org/10.1016/j.molliq.2020.112598.

References

[1] J.B. Hasted, Liquid water: dielectric properties, in: F. Franks (Ed.), Water A Comprehensive Treatise, 1, Plenum Press, New York, 1972, pp. 255–309.
[2] K. Ichikawa, Y. Kameda, T. Yamaguchi, H. Wakita, M. Misawa, Neutron-diffraction investigation of the intramolecular structure of a water molecule in the liquid phase at high temperatures, Mol. Phys. 73 (1991) 79.
[4] J.S. Kim, A.R. Morrow, A. Yethira, A. Yethiraj, Self-diffusion and viscosity in electrolyte solutions, J. Phys. Chem. B. 116 (2012) 12007–12013.
[5] Y.J. Wu, H.L. Tepper, G.A. Voth, Flexible simple point-charge water model with improved liquid-state properties, J. Chem. Phys. 124 (024503). (2006)
[6] M.A. González, J.L.F. Abascal, A flexible model for water based on TIP4P/2005, J. Chem. Phys. 135 (224516-). (2011)
[7] L. Barrat, I.R. McDonald, The role of molecular flexibility in simulations of water, Mol. Phys. 70 (1990) 535–539.
[8] D.E. Smith, A.D.J. Haymet, Structure and dynamics of water and aqueous solutions: the role of flexibility, J. Chem. Phys. 96 (1992) 8450–8459.
[9] C. Vega, J.L.F. Abascal, Simulating water with rigid non-polarizable models: a general perspective, Phys. Chem. Chem. Phys. 13 (2011) 19663–19688.
[10] A. Warshel, Computer Modeling of Chemical Reactions in Enzymes and Solutions, J. Wiley & Sons, Inc., New York, 1991.
[11] U.W. Schmitt, G.A. Voth, Multistate empirical valence bond model for proton transport in water, J. Phys. Chem. B. 102 (1998) 5547–5551.
[12] U.W. Schmitt, G.A. Voth, The computer simulation of proton transport in water, J. Chem. Phys. 111 (1999) 9361–9381.
[13] J. López-Lemus, G.A. Chapela, J. Alejandre, Effect of flexibility on surface tension and coexisting densities of water, J. Chem. Phys. 128 (174703). (2008)
[14] R. Fuentes-Azcatl, N. Mendoza, J. Alejandre, Improved SPC force field of water based on the dielectric constant: SPC/ε, J. Physica A. 420 (2015) 116–123.
[15] S. Izadi, A.V. Onufriev, Accuracy limit of rigid 3-point water models, J. Chem. Phys. 145 (074501). (2016)
[16] R. Fuentes-Azcatl, M.C. Barbosa, Thermodynamic and dynamic anomalous behavior in the TIP4p/ϵ water model, Physica A. 444 (2016) 86–94.
[17] R. Fuentes-Azcatl, H. Dominguez, Prediction of experimental properties of CO_2: improving actual force fields, J. Mol. Modeling. 25 (2019) 146.
[18] R. Fuentes-Azcatl, J. Alejandre, Non-polarizable force field of water based on the dielectric constant: TIP4p/ϵ, J. Phys. Chem. B. 118 (2014) 1263–1272.
[19] B. Hess, C. Kutzner, D. van der Spoel, E. Lindahl, GROMACS 4.5 Algorithms for highly efficient, load-balanced, and scalable molecular simulation, J. Chem. Theory Comput. 4 (2008) 435–447.
[20] D. van der Spoel, E. Lindahl, B. Hess, G. Groenhof, A.E. Mark, H.C. Berendsen, GROMACS: fast, flexible, and free, J. Comput. Chem. 26 (2005) 1701–1718.
[21] M. Parrinello, A. Rahman, Polymorphic transitions in single crystals: a new molecular dynamics method, J. Appl. Phys. 52 (1981) 7182–7190.
[22] U. Essmann, L. Perera, M.L. Berkowitz, T. Darden, H. Lee, L.G. Pedersen, A smooth particle mesh Ewald method, J. Chem. Phys. 103 (1995) 8577–8592.
[23] J.P. Hansen, I.R. McDonald, Theory of Simple Liquids, 4th ed. ed., Elsevier, Amsterdam, 2013.
[24] M. Neumann, Dipole moment fluctuation formulas in computer simulations of polar systems, Mol. Phys. 50 (1983) 841–845.
[25] A. Truckymchuk, J. Alejandre, Computer simulations of liquid/vapor interface in Lennard-Jones fluids: some questions and answers, J. Chem. Phys. 111 (1999) 8510–8523.
[26] P. Orea, J. López-Lemus, J. Alejandre, Oscillatory surface tension due to finite–size effects, J. Chem. Phys. 123 (2005) 114702–114813.
[27] M. Gonzalez-Melchor, F. Bresme, J. Alejandre, Molecular dynamics simulations of the surface tension of ionic liquids, J. Chem. Phys. 122 (2005) 104710–104718.
[28] R. Garcia Fernández, J.L. Abascal, C. Vega, The melting point of ice Ih for common water models calculated from direct coexistence of the solid-liquid interface, J. Chem. Phys. 124 (144506). (2006)
[29] V.F. Petrenko, R.W. Whitworth, Physics of Ice, Oxford University Press, Oxford, 1999.
[30] A. Zeidler, P. Salmon, H.E. Fischer, J.C. Neuefeind, J.M. Simonson, T.E. Markland, Isotope effects in water as investigated by neutron diffraction and path integral molecular dynamics, J. Phys. Condens. Matter 24 (284126). (2012)
[31] A.H. Narten, H.A. Levy, Liquid water: molecular correlation functions from X ray diffraction, J. Chem. Phys. 55 (1971) 2263–2269.
[32] B. Tomberli, C.J. Benmore, P.A. Egelstaff, J. Neuefeind, V. Honkimaki, Isotopic quantum effects in water structure measured with high energy photon diffraction, J. Phys. Condens. Matter. 12 (2000) 2597–2612.
[33] M. Chaplin, Structure, function, behavior and properties of water, http://www.lsbu.ac.uk/water, Accessed date: 1 June 2018.
[34] E.W. Lemmon, M.O. McLinden, D.G. Friend, Thermophysical Properties of Fluid Systems, NIST Chemistry WebBook, NIST Standard Reference Database, in: P.J. Linstrom, W.G. Mallard (Eds.), 2005, http://webbook.nist.gov, Accessed date: 1 July 2018.
[35] P.F. Prini, International Association for the Properties of Water and Steam, http://www.iapws.org/relguide/IF97-Rev.pdf, 2007, Accessed 1 June 2018.
[36] R.G. Fernández, J.L.F. Abascal, C. Vega, The melting point of ice i for common water models calculated from direct coexistence of the solid-liquid interface, J. Chem. Phys. 124 (2006) 144506–144518.
[37] C. Vega, J.L.F. Abascal, M.M. Conde, J.L. Aragones, What ice can teach us about water interactions: a critical comparison of the performance of different water models, Faraday Discuss. 141 (2009) 251–276.

Further Reading

[3] A. Furlan, E. Lomba, M.C. Barbosa, Temperature of maximum density and excess properties of short-chain alcohol aqueous solutions: a simplified model simulation study, J. Chem. Phys. 146 (144503). (2017)